

## 40 Hz Electroacupuncture relieves the memory dysfunction of 5xFAD mice by regulating neuronal electrical activity

Jifei Miao<sup>\*</sup>, Xiaoming Liu, Jiao Lan<sup>\*</sup>

Shenzhen Bao'an Traditional Chinese Medicine Hospital, Shenzhen, China



### ARTICLE INFO

**Keywords:**  
Electroacupuncture  
Alzheimer's Disease  
Neural oscillation  
Synaptic transmission  
 $\text{A}\beta$

### ABSTRACT

In this investigation, we probed the impacts of 40 Hz Electroacupuncture (EA) on the cognitive function and brain activity in 5xFAD mice. Three groups of mice were constituted: the Model group of 5xFAD mice, the Wild Type (WT) group of littermate controls, and the EA group of 5xFAD mice subjected to EA treatment. Behavioral tests were conducted to evaluate memory function and anxiety levels, while the presence of  $\text{A}\beta$  plaques were detected via immunostaining, and neuronal activity was measured using multichannel recordings. Our results indicated that EA therapy enhanced memory function and anxiety-like behavior in 5xFAD mice, as well as diminishing the abundance and dimensions of  $\text{A}\beta$  plaques in the hippocampus and mPFC regions. Notably, the suppression of astrocyte activation was observed, which was potentially associated with alterations in gamma oscillation. Furthermore, the synaptic transmission of neurons was amplified, suggesting a possible modulation in neural activity. These findings indicate that 40 Hz EA could influence cognitive performance and potentially affect neuronal activity in 5xFAD mice, while the direct connection between EA and neuronal electrical activity regulation requires further exploration. The potential frequency-specific effects of EA on protective mechanisms in the brain was not addressed in this study and thus presents a direction for future research.

### 1. Introduction

Alzheimer's disease (AD) is a prevalent neurodegenerative disorder initially marked by learning and memory impairment, later progressing to language disorder and disorientation. More than 40 genes have been implicated in AD (Scheltens et al., 2022); many involved in  $\text{A}\beta$  and Tau hyper-phosphorylation, such as APP (Zhao et al., 2020), PS1 (Bustos et al., 2021) and APOE (Parhizkar and Holtzman, 2022). The primary treatment strategy has been  $\text{A}\beta$  elimination. Still, drugs like Aducanumab and BAN2401, which target  $\text{A}\beta$ , have not yielded significant therapeutic results (van Dyck, 2018; Sevigny et al., 2016). Interestingly, acupuncture, a technique from traditional Chinese medicine, has demonstrated effectiveness in treating AD (Xie et al., 2021; Zheng et al., 2021), warranting a closer look at its mechanism of action.

Neuronal defects hold a pivotal role in the onset of AD. The demise and dysfunction of synapses, the fundamental units of neurons, directly correlate with cognitive impairment in AD patients (Peng et al., 2022). Alterations in the number and morphology of synapses in the hippocampus of both AD patients and model rats have been observed (Colom-Cadena et al., 2020). Moreover, there is a documented decrease in

excitatory postsynaptic current (EPSC) (He et al., 2019) and inhibitory postsynaptic current (IPSC) (Ruiter et al., 2020), alongside attenuated long-term potentiation (LTP) (Diociaiuti et al., 2021) and long-term depression (LTD) (D'Amelio et al., 2011; Lanté et al., 2015). Evidence suggests that EA can improve cognitive function by modulating synaptic plasticity, LTP, and LTD (Ye et al., 2017; Xiao et al., 2018; Tang et al., 2019). However, the precise mechanism remains elusive and demands further exploration.

Neural oscillations, rhythmic activities of neurons within the central nervous system, are essential for various cognitive processes, including learning and memory (Doelling and Assaneo, 2021). These oscillations span from slow delta (0.5–3 Hz) to fast gamma (30–100 Hz) and ultrafast (100–200 Hz) frequencies. In AD, the neural oscillations' disruption leads to the loss of gamma oscillations-dominated activity, culminating in memory and cognitive defects (Arroyo-García et al., 2021). Reinstating gamma oscillations' activity has demonstrated a reduction in  $\text{A}\beta$  production, facilitated the clearance of  $\text{A}\beta$  plaques, and enhanced memory and cognitive functions (Etter et al., 2019; Iaccarino et al., 2016). Notably, a study by Li-Huei Tsai from MIT revealed that 40 Hz light and sound stimulation could synchronize gamma oscillations,

\* Corresponding authors.

E-mail address: [505970191@qq.com](mailto:505970191@qq.com) (J. Lan).

reduce A $\beta$  and Tau protein concentrations, and augment memory function in mice (Martorell et al., 2019).

This study's primary objective was to examine the effect of 40 Hz EA stimulation on memory impairment, A $\beta$  plaques, gamma oscillations, and synaptic function in mice. Our findings indicated that 40 Hz EA stimulation significantly ameliorated memory impairment, reduced A $\beta$  plaque levels, decreased abnormally heightened gamma oscillations, and improved the function of excitatory synapses in mice. These results suggest that 40 Hz EA stimulation could potentially enhance gamma oscillations, thereby offering a novel therapeutic avenue for AD. To substantiate these findings and gain a deeper understanding of the underlying mechanisms, further research is imperative.

## 2. Methods

### 2.1. Mice

In this research, we engaged eight-week-old female C57BL/6 mice from the Animal Laboratory Centre of Guangdong Province in Guangzhou, China, for breeding. These mice also doubled as littermate controls for 3xTg and 5xFAD mice, ensuring a unified genetic background and environmental conditions across all groups. The 3xTg and 5xFAD transgenic mouse strains, recognized as models for AD, were kindly donated by the Shenzhen Center for Disease Control and Prevention. The 3xTg strain bears mutations in three genes (APPswe, PS1M146V, and tauP301L) that engender Alzheimer's-like symptoms such as plaques, tangles, cognitive deficits, and neuronal loss. Conversely, the 5xFAD strain carries five familial AD mutations, instigating robust, early-onset amyloid pathology in the brain. From these strains, we selected 4–5-month-old mice for experimentation. They were kept in a specific pathogen-free laboratory with controlled conditions—22 °C temperature and 50%–70% humidity—and granted free access to food and water while following a 12-hour light/dark cycle. The Guangzhou University of Traditional Chinese Medicine's Institutional Animal Care and Use Committee's guidelines directed all experimental proceedings.

### 2.2. EA treatment

In this study, 4–5 month-old 5xFAD mice were randomly divided into two groups: the EA group and the Model group, with the littermate control mice serving as the control group. The mice in the EA group were anesthetized with isoflurane to maintain comfort and minimize movement during the treatment. They were then immobilized using a stereotaxic instrument to ensure precise placement of the stainless steel needles into the acupoints "Baihui" (GV20) and "Dazhui" (GV14).

The needles were stimulated with a current intensity of 1 mA at a frequency of 40 Hz, which was sustained for a duration of 30 min. This treatment was repeated once daily for a total of 21 days. During the entire EA procedure, the mice remained under anesthesia to prevent any disruption of the needles' position. Special precautions were taken to ensure that the needles remained in place and were not disturbed by the mice.

On the other hand, the mice in the control and Model groups were not subjected to any treatments, but were maintained under the same conditions for comparison purposes. It should be noted that all experimental procedures were approved by the Institutional Animal Care and Use Committee of Guangzhou University of Traditional Chinese Medicine, ensuring ethical conduct of the research.

### 2.3. Open field experiment

Mice were analyzed for anxiety-like behavior by placing them in a square field (45 cm × 45 cm × 45 cm) that was divided into 16 smaller squares. The mice were initially placed in the center square, and their movements were tracked and recorded using Viewer software (Biobserve GmbH, Germany). This software allowed us to collect

comprehensive data on path movement, speed, and distance traveled. The behavioral tests were conducted under dim light conditions during the day, two days after the EA treatment, to ensure that the immediate effects of the treatment had dissipated.

### 2.4. Fear conditioning experiment

We assessed the impact of EA on the fear memory of mice through the analysis of their freezing behavior. During the training phase, the mice were introduced to a fear conditioning box for 2 min, during which their baseline freezing time was recorded. Following this, a sound stimulus (80 dB, 30 s) was presented, followed by an electric shock (0.35 mA, 2 s). On the next day, a context test and a cued test were conducted using the Freeze Frame system and Freeze View analysis software from Coulbourn Instruments. For the cued test, a triangular chamber was placed within the original context test chamber, and to eliminate any residual odor from the context test, a drop of fruit juice was smeared in the box. The freezing behavior in response to the sound stimulus was recorded, and the differences among the groups were analyzed to evaluate the effect of EA on fear memory.

### 2.5. Novel object recognition experiment

We examined the effect of EA on the recognition memory of mice through an object recognition test. In this test, two identical objects (A and B) were placed at opposite ends of an open box. The mice, placed with their backs facing the objects, were allowed to explore the objects, and their interactions were recorded using the Viewer software (Biobserve GmbH, Germany). Following a 10-minute exploration period, the mice were removed and reintroduced to the box an hour later, but this time, a new object (C) replaced object B. Their exploration of the new object was recorded over a 5-minute period. Differences in the exploration of the new object among the groups were compared to assess the impact of EA on recognition memory. The discrimination index was calculated using the following formula: (Time spent with novel object - Time spent with familiar object) / (Time spent with novel object + Time spent with familiar object).

## 3. 3-Chamber experiment

Additional details regarding the 3-chamber experiment are as follows. The apparatus consisted of a box divided into three equal compartments with openings allowing free access among them. The test mouse was initially placed in the central chamber, while an unfamiliar mouse (stranger 1) was located in a wire cage in one of the side chambers, and an empty wire cage was in the other side chamber. The amount of time the test mouse spent in each chamber was recorded. In the second phase, another unfamiliar mouse (stranger 2) was placed in the previously empty cage. The time spent by the test mouse in each chamber was recorded again. The relative time spent with stranger 1 and stranger 2 provided a measure of social memory. This test was conducted under similar conditions as the previously described tests.

### 3.1. Electrode embedding and multichannel recording

During the experiment, mice were anesthetized via inhalation of isoflurane, administered in a mixture with oxygen. Once the mice were adequately anesthetized, they were positioned in a stereotaxic frame. Operating under aseptic conditions, a midline incision was made to expose the skull, and the coordinates for the CA1 region of the hippocampus were determined based on the mouse brain atlas (Anteroposterior, -2.0 mm; Mediolateral, +/-1.5 mm; Dorsoventral, -1.5 mm). We employed a custom-built multichannel electrode, manufactured from insulated stainless-steel wires, to locate and record the spike signal from this region. The electrode was carefully lowered to the specified depth, and the field potential waveforms were monitored to

ensure proper positioning. Once a stable signal was obtained, the electrode was secured in place with dental acrylic, and the surgical site was sutured. To prevent any potential brain tissue damage, paraffin oil was applied to cover the electrode. After a recovery period of four days, the multichannel signal acquisition system was connected to the electrode for data collection. The recorded field potentials and neuronal electrical signals were then filtered, sampled, and subsequently analyzed using Offline Sorter, NeuroExplorer, and MATLAB software.

### 3.2. Preparation of acute brain slices

Before beginning, it is necessary to prepare the slicing fluid and the artificial cerebrospinal fluid (ACSF). The composition of the slicing fluid consists of: 125 mM NaCl, 2.5 mM KCl, 3 mM MgCl<sub>2</sub>, 0.1 mM CaCl<sub>2</sub>, 25 mM glucose, 1.25 mM NaHPO<sub>4</sub>, 25 mM NaHCO<sub>3</sub>, 0.4 mM ascorbic acid, 3 mM myo-inositol, and 2 mM sodium pyruvate. The composition of the ACSF is similar and consists of: 125 mM NaCl, 2.5 mM KCl, 1 mM MgCl<sub>2</sub>, 2 mM CaCl<sub>2</sub>, 25 mM glucose, 1.25 mM NaHPO<sub>4</sub>, 25 mM NaHCO<sub>3</sub>, 0.4 mM ascorbic acid, 3 mM myo-inositol, and 2 mM sodium pyruvate. Both fluids are balanced to have a pH of 7.4.

The slicing fluid is frozen in an ice-water mixture and continuously filled with a 95% O<sub>2</sub> and 5% CO<sub>2</sub> mixture for 15 min to achieve oxygen saturation. The mice are then anesthetized with isoflurane and promptly placed in the oxygenated slicing fluid. The skull is meticulously dissected and the posterior part of the brain is cut off using a coronal plane and attached to the slicing platform. The slices are made using a vibrating microtome under continuously oxygenated ice-cold conditions. The thickness of the slices for the hippocampus is 300 mm and for the prefrontal cortex is 250 mm. Finally, the brain slices containing the largest cross-section of the hippocampus or prefrontal cortex are placed in ACSF at 32°C that has been oxygenated for over 30 min, and then brought to room temperature for later use.

### 3.3. Whole-cell patch-clamp

The resistance of the recording pipette was maintained at 3–5 MΩ. The internal solution for EPSC recordings consisted of 117 mM Cs-methanesulfonate, 15 mM CsCl, 8 mM NaCl, 10 mM TEA-Cl, 0.2 mM EGTA, 4 mM Na<sub>2</sub>-ATP, 0.3 mM Na<sub>2</sub>-GTP, and 10 mM HEPES, with pH adjusted to 7.3 using CsOH. EPSCs in the CA1 region of the hippocampus were elicited by administering current stimulations at intensities of 20 mA, 40 mA, 60 mA, 80 mA, and 100 mA in the CA3 region, under a whole-cell voltage clamp at a holding potential of -70 mV. Similarly, to elicit EPSCs in the L5/6 pyramidal neurons of the prefrontal cortex, the same current stimulation intensities were applied to the L2/3 region. In addition to evoked EPSCs, we also recorded miniature EPSCs (mEPSCs) from the CA1 region of the hippocampus and the L5/6 region of the prefrontal cortex. The recordings were conducted at a holding potential of -70 mV. To isolate AMPA receptor-mediated EPSCs, 50 μM picrotoxin (PTX) was added to the artificial cerebrospinal fluid (ACSF). Miniature EPSCs were recorded in the presence of 50 μM PTX and 0.5 μM TTX. For the recording of NMDA receptor-mediated EPSCs, ACSF was supplemented with 50 μM PTX and 10 μM CNQX. The synaptic transmission function was characterized by analyzing various EPSC parameters such as frequency and amplitude. Meanwhile, miniature inhibitory postsynaptic currents (mIPSCs) were also recorded in separate sessions. All electrophysiological data were collected using an Axon Multiclamp 700B patch-clamp amplifier and an Axon Digidata 1440A digital-to-analog converter, filtered at 1 kHz and sampled at 10 kHz. Data analysis was conducted using Clampfit 10.7 software.

### 3.4. Immunofluorescence staining

The experimental mice were deeply anesthetized with isoflurane and perfused with 0.1 M PBS + 4% PFA. After the mice were fixed, the brains were dissected and fixed in 4% PFA for 12 h, then transferred to 30%

sucrose solution for dehydration for 48 to 72 h. After embedding in O.C.T., coronal sections were sliced on a freezing microtome with a thickness of 30 μm. The brain slices with the largest cross-section were washed three times in 0.1 M PBS for 10 min each and then treated with a blocking solution containing 0.3% Triton-X100 and 5% BSA for 30 min at room temperature to permeabilize the membranes and block non-specific binding. The primary antibodies, including anti-GFAP (abcam, ab7260, 1:1000) and anti-Aβ (abcam, ab201060, 1:1000), were incubated overnight at 4 °C. After the overnight incubation, the sections were washed three times with 0.1 M PBS for 10 min each time. Staining labeling was performed by incubating with fluorescent secondary antibodies for 1 h in the dark at room temperature. The sections were washed three times with 0.1 M PBS for 10 min each time after the labeling. The images were captured using a Nikon A1R laser confocal microscope. Fluorescence images were taken with a 40x oil lens at a thickness of 10 μm.

### 3.5. Quantification and statistical analysis

The data presented in the report are expressed as the average ± standard error of the mean (SEM), and the significance of the results was evaluated using statistical tests such as Student's *t*-test, two-way analysis of variance (ANOVA), or Kolmogorov-Smirnov test. Results with a significance level of \**P* < 0.05, \*\**P* < 0.01, \*\*\**P* < 0.001, and \*\*\*\**P* < 0.0001 are considered statistically significant, while results with *P* greater than 0.05 are not specifically highlighted.

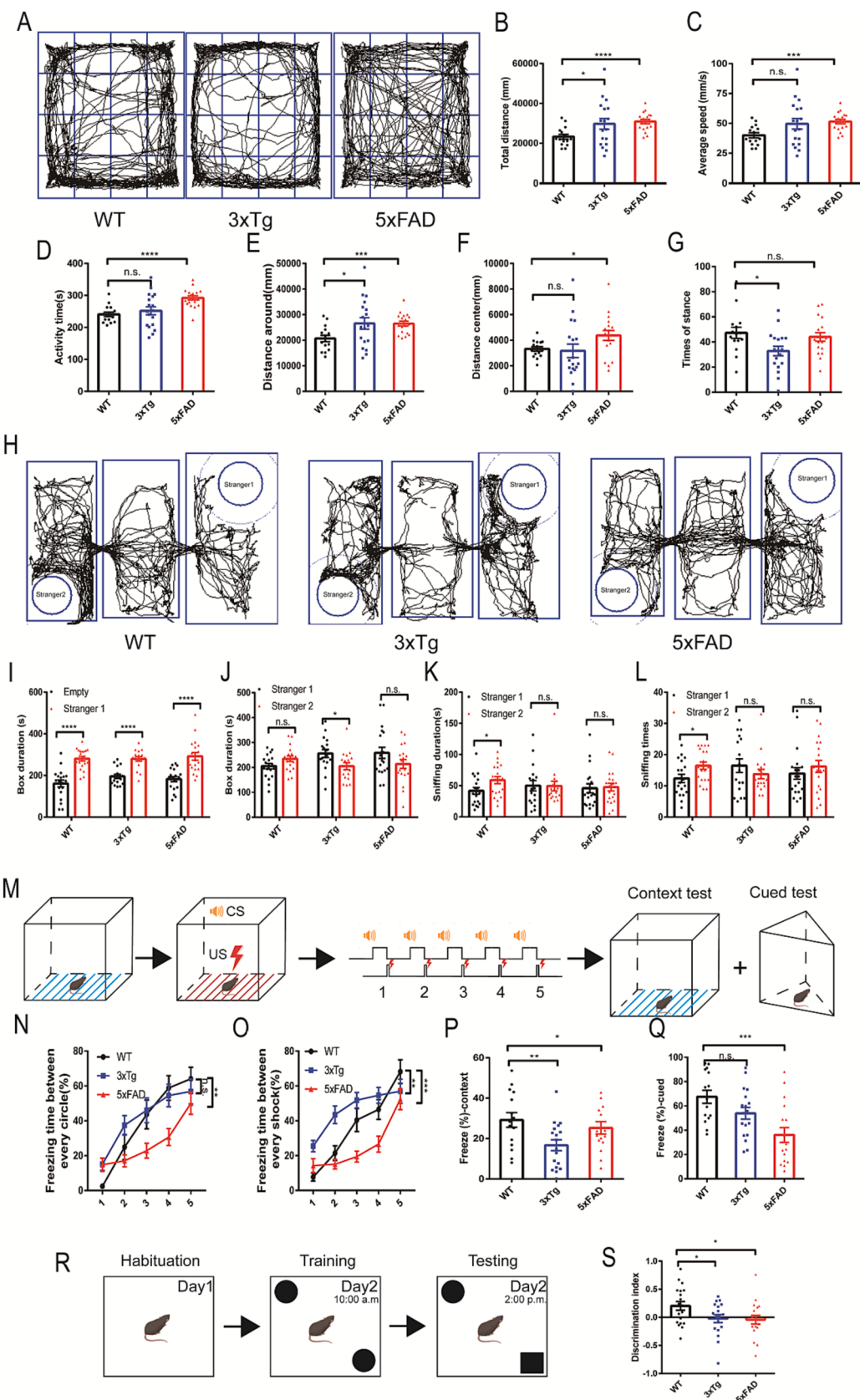
## 4. Result

### 4.1. 5xFAD mice showed severe memory impairment

In order to identify the most suitable AD model for our investigation, we assessed the memory and anxiety levels of 3xTg and 5xFAD mice. The control group consisted of unmodified C57BL/6 mice. Using an open field test, we examined total distance traveled, average speed, and activity duration in each mouse model. The 5xFAD mice exhibited an increase in all these measures compared to the control group (Fig. 1A-D). Interestingly, only the 3xTg mice covered a greater distance than the control group (Fig. 1B). In terms of the central area of the open field, marked by the middle four squares, 5xFAD mice traveled extensively in both central and peripheral zones. On the other hand, 3xTg mice primarily covered longer distances in the peripheral area (Fig. 1E and F). Despite the 3xTg mice displaying fewer stances than the control group (Fig. 1G), our findings suggest a decreased anxiety-like behavior in 5xFAD mice.

In a two-stage, three-chambered experiment, we evaluated the social ability and memory of WT, 3xTg, and 5xFAD mice. The amount of time spent in the sections containing either an empty space or a stranger mouse (stranger 1) was documented. All three mouse groups displayed similar social behaviors, primarily interacting with stranger 1 instead of remaining in the empty section, indicating intact social abilities (Fig. 1H, I). In the second phase, a new mouse (stranger 2) was introduced and we recorded the time spent by each mouse in the compartments with either stranger 1 or stranger 2. Both 3xTg and 5xFAD mice spent less time with stranger 2, and no distinct differences were noted in sniffing duration or frequency between the strangers. This implies a notable reduction in social memory in the 3xTg and 5xFAD mice, further validated by comparisons with the WT group that showed an inclination towards interacting with stranger 2 (Fig. 1H, J-L). These results highlight a deficiency in social memory in 3xTg and 5xFAD mice.

In a fear conditioning experiment, we evaluated the fear responses of the mice by measuring the freezing time between shocks or circles. The 5xFAD mice exhibited a shorter freezing time compared to 3xTg mice, who only demonstrated this effect between shocks (Fig. 1N and O). Subsequent fear memory tests also indicated that 5xFAD mice had a more substantial impairment in fear memory than the 3xTg mice,



(caption on next page)

**Fig. 1.** 5xFAD mice showed more significant memory impairment (A) Trajectory chart of open field experiments. (B) Analysis of the results of the total distance of the open field experiment. (C) Analysis of the results of the average speed of the open field experiment. (D) Analysis of the results of the activity time of the open field experiment. (E) Analysis of the results of the distance around the open field experiment. (F) Analysis of the results of the distance center of the open field experiment. (G) Analysis of the results of the times of stance of the open field experiment. (H) Trajectory chart of 3-chamber experiments. (I) Analysis of the results of the duration mice spend in different areas (empty and stranger1) of the 3-chamber experiment. (J) Analysis of the results of the duration mice spends in different areas (stranger 1 and stranger 2) of the 3-chamber experiment. (K) Analysis of the results of the sniffing duration mice contact with different strangers of the 3-chamber experiment. (L) Analysis of the results of the sniffing times mice contact with different strangers of the 3-chamber experiment. (M) Schematic diagram of the fear conditioning experiment. (N) Analysis of the results of the freezing time between every cycle of the fear conditioning experiment. (O) Analysis of the results of the freezing time between every shock of the fear conditioning experiment. (P) The freezing ratio in context test. (Q) The freezing ratio in the cued test. (R) Schematic diagram of the novel objective recognition experiment. (S) Analysis of the results of the novel objective recognition experiment. All data are means  $\pm$  SEM. N = 15 in the WT group, n = 18 in both 3xTg and 5xFAD groups. Statistical significance was assessed by unpaired two-tailed t-test or two-way ANOVA (\* $P < 0.05$ , \*\* $P < 0.01$ , \*\*\* $P < 0.001$ , \*\*\*\* $P < 0.0001$ ).

leading us to select the 5xFAD mice for further testing due to their pronounced memory deficits.

We further probed memory capabilities by conducting a novel object recognition experiment. Here, the WT group demonstrated a clear preference for the new object, spending a significant amount of time near it. In stark contrast, both 3xTg and 5xFAD mice exhibited a decreased preference for the novel object (Fig. 1R and S). This finding indicates severe object memory deficits in both 3xTg and 5xFAD mice, suggesting impaired novelty recognition.

#### 4.2. EA alleviated the memory impairment of 5xFAD mice

Following 21 days of 40 Hz electrical stimulation at the Baihui and Dazhui acupoints (Fig. 2A), we assessed the impact of this treatment on the anxiety levels of the 5xFAD mice. The findings demonstrated that the 5xFAD mice covered more extensive distances in the central area, dedicated more time in this central zone, and moved at faster average speeds compared to the control group. Notably, these behavioral traits were reversed post the electrical stimulation (Fig. 2A-C), which suggests that the electrical stimulation method might have amplified the anxiety-

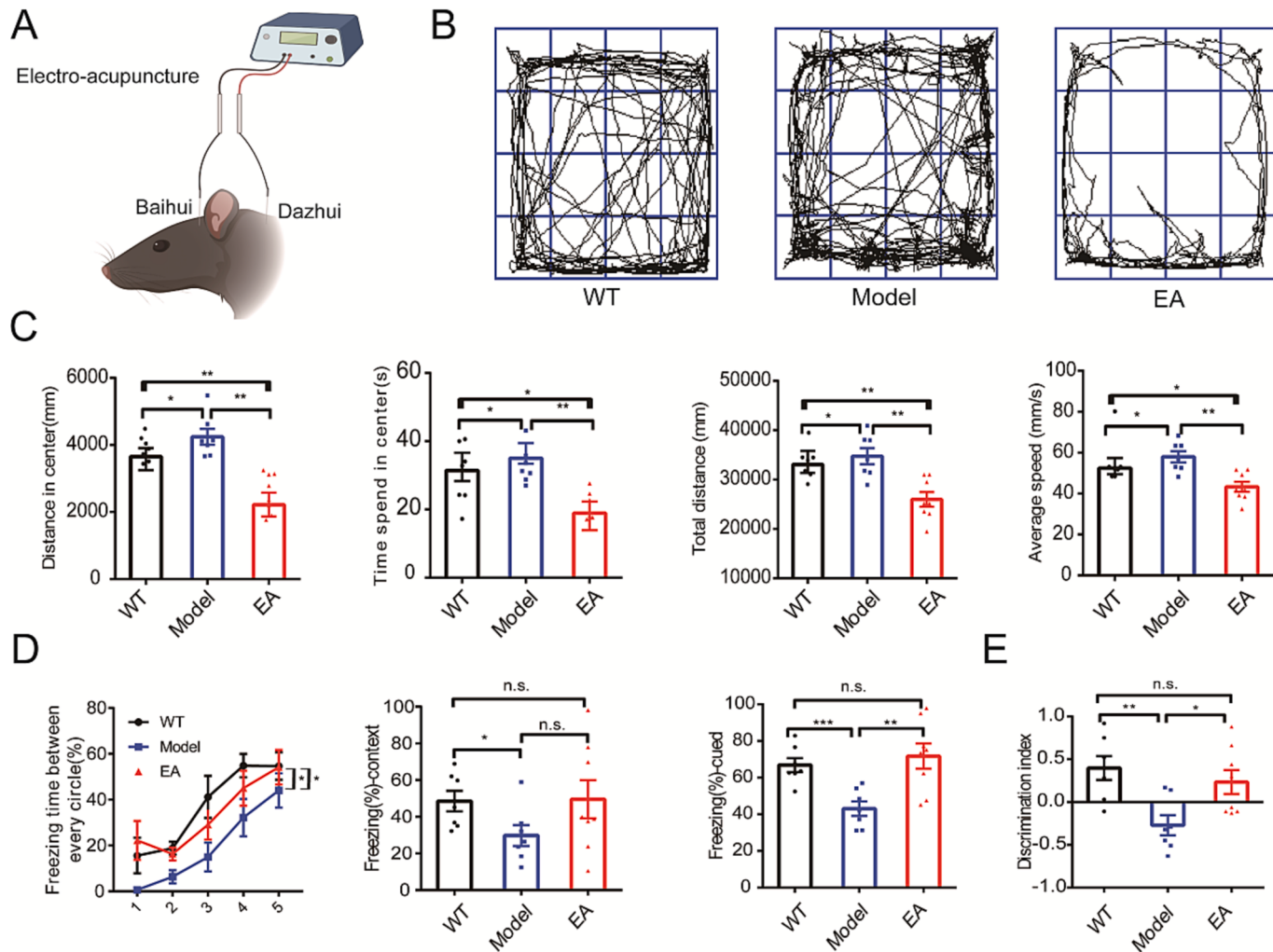


**Fig. 2.** EA alleviates the memory impairment of 5xFAD mice (A) Schematic diagram of EA stimulation of Baihui and Dazhui acupoints. (B) Trajectory chart of open field experiments. (C) EA reduced the total distance, average speed, distance in the center, and time spent in the center of 5xFAD mice in the open field test. (D) EA improved the fear memory of 5xFAD mice, including the freezing time between every cycle, and the freezing time in the cued test, but not the freezing time in the context test. (E) EA improved the recognition ability of 5xFAD. All data are means  $\pm$  SEM. N = 7 in both WT and Model groups, n = 8 in the EA group. Statistical significance was assessed by unpaired two-tailed t-test or two-way ANOVA (\* $P < 0.05$ , \*\* $P < 0.01$ , \*\*\* $P < 0.001$ , n.s. = not significant).

like behavior manifested by the 5xFAD mice.

Subsequently, we engaged a fear conditioning experiment to inspect the influence of electrical stimulation on the fear memory of the 5xFAD mice. The data revealed that the electrical stimulation resulted in an elongation of the freezing time exhibited by the 5xFAD mice during each cycle and in the cued test. Although there was no detectable difference between the control group and the electrically stimulated group in the context test, an upward trend was observed in the electrical stimulation group when compared to the control (Fig. 2D). The control and electrically stimulated groups presented no differences in both the context and cued tests. These findings hint that the electrical stimulation might have bolstered the fear memory of the 5xFAD mice.

Lastly, we conducted a novel object recognition experiment to investigate the effects of electrical stimulation on the object memory of the 5xFAD mice. The results indicated that the electrical stimulation enhanced the object recognition memory in the 5xFAD mice (Fig. 2E).

#### 4.3. EA reduced the amount of A $\beta$ in the brain of 5xFAD mice

Our objective was to explore the influence of EA on the presence of A $\beta$  plaques in 5xFAD mice, following earlier findings of EA's beneficial effects on the memory of these mice. In order to quantify the number and size of the plaques, A $\beta$  plaques were stained and tallied within the hippocampus and the mPFC regions (Fig. 3A and E). In parallel, we evaluated astrocyte activity through GFAP staining (Fig. 3A and E). Our findings demonstrated that, compared to wild-type mice, 5xFAD mice exhibited higher GFAP intensity, a greater quantity of A $\beta$  plaques, and larger plaque size. After 21 days of 40 Hz EA stimulation on the Baihui and Dzhui acupoints, the GFAP intensity in the hippocampus decreased from 1.2 to 0.8 (Fig. 3B). In addition, the quantity of A $\beta$  plaques reduced from 20 to 15 (Fig. 3C), alongside a decrease in plaque size from 5000 to 3500 (Fig. 3D). In the mPFC region, a similar trend was observed. The EA stimulation led to a decrease in GFAP intensity from 1.3 to 0.7 (Fig. 3F), the quantity of A $\beta$  plaques reduced from 12 to 8 (Fig. 3G), and the size of the plaques diminished from 4400 to 3000 (Fig. 3H). These findings suggest that 40 Hz EA stimulation has the potential to reduce both astrocyte activation and the number and size of A $\beta$  plaques.

#### 4.4. EA inhibited the high-frequency gamma oscillations in the hippocampus and PFC region of 5xFAD mice

Earlier research indicated that 40 Hz light and sound stimulation could minimize the number and size of A $\beta$  plaques by amplifying gamma oscillation. Thus, we examined the effect of 40 Hz EA stimulation on LPF, gamma, and theta oscillations in both the hippocampus and PFC region. Contrary to previous findings, we noticed an elevation in LPF, high gamma, and low gamma oscillations in the hippocampus of the 5xFAD mice (Fig. 4A-E). However, EA proved effective in curbing the abnormal increase in high gamma oscillation, though it did not significantly impact low gamma oscillation. This hints that 40 Hz EA is capable of restoring the oscillation intensity back to normal levels, primarily impacting the high gamma oscillation. We observed no significant change in theta oscillation across all three groups (Fig. 4F,G). In the PFC region, like in the hippocampus, there were elevated LPF, high gamma, and low gamma oscillations in 5xFAD mice (Fig. 4H-L), while theta oscillation was reduced (Fig. 4M,N). Similar to the hippocampus, EA managed to hinder the excessive increase in high gamma oscillation, but not low gamma or theta oscillation, in the PFC region (Fig. 4N). These results suggest that EA effectively mitigated high gamma oscillations in both the hippocampus and PFC regions of 5xFAD mice.

#### 4.5. EA enhanced synaptic transmission in 5xFAD mice

In order to investigate the connection between neural oscillations and synaptic transmission functionality, we executed a whole-cell patch-clamp experiment. This was done to evaluate the synaptic transmission

of pyramidal neurons in both the hippocampus and the mPFC region. Initially, we tested the mEPSC in the hippocampus. When compared to the control group of wild-type mice, both the frequency and amplitude of mEPSC in the experimental 5xFAD mice were reduced. Additionally, both the decay time and rise time were extended. However, these reductions were mitigated by electrical stimulation (EA), which significantly increased the frequency and amplitude of mEPSC, while decreasing the rise time (Fig. 5A).

Similarly, the mIPSC in the hippocampus of 5xFAD mice showed a decrease in amplitude, frequency, and rise time, and an increase in decay time. The application of EA improved the frequency, decay time, and rise time, although it didn't significantly impact the amplitude (Fig. 5B). Considering that EA had improved the amplitude and frequency of mEPSC in the CA1 region, we then sought to examine its influence on neurotransmission from the CA3 to CA1 region. We applied depolarizing currents of 20 mA, 40 mA, 60 mA, 80 mA, and 100 mA in the CA3 region and registered the EPSC in the CA1 region (Fig. 5C). Our findings showed that both AMPA and NMDA-mediated transmissions were reduced in 5xFAD mice, but EA notably increased the AMPA-mediated EPSC (Fig. 5D). Although no significant difference was observed in the NMDA-mediated EPSC after EA stimulation, an obvious trend of increased amplitude was evident (Fig. 5E).

In the mPFC region, both mIPSC and mEPSC in the 5xFAD mice displayed a reduction in amplitude and frequency, with an increase in both decay time and rise time, when compared to the wild-type mice. Nevertheless, EA rescued the decreases in amplitude and frequency, as well as the increases in rise time for both mEPSC and mIPSC (Fig. 5F,G). To assess neural transmission in the mPFC region, we applied depolarizing currents of 20 mA, 40 mA, 60 mA, 80 mA, and 100 mA in L2/3 and recorded the EPSC at L5/6 (Fig. 5H). Both AMPA and NMDA mediated EPSC were reduced in the model group but saw an increase in the EA group (Fig. 5 I,J). These findings collectively suggest that EA could enhance synaptic transmission in 5xFAD mice.

## 5. Discussion

EA as a traditional treatment method in Chinese Medicine has garnered considerable attention in both clinical and laboratory research. Studies have demonstrated that EA is effective in managing AD by lowering levels of A $\beta$  (Zheng et al., 2021), phosphorylated Tau protein (D'Amelio et al., 2011; Xu et al., 2020), enhancing cell autophagy (Zheng et al., 2020), and enhancing synaptic plasticity (Yang et al., 2020). However, the effects of EA on neuronal electrical activity remain to be fully understood. To gain deeper insights, we carried out behavioral research, multichannel recording, and whole-cell patch-clamp experiments to ascertain if EA can alleviate memory dysfunction through the regulation of electrical activity.

Our initial objective was to identify the most suitable AD mouse model for our research. Here, we contemplated 5xFAD and 3xTg mice, common choices in AD mouse model studies. The 5xFAD mice have three mutant sites on the APP695 gene (K670N/M671L, I716V, and V717I) and two on the PS1 gene (M146L and L286V). Beginning at 1.5 months old, 5xFAD mice display endogenous A $\beta_{42}$  accumulation in brain neurons and axons. By 2 months, amyloid deposition starts in the hippocampus, accompanied by gliosis and memory impairment, which correlates with decreased synaptic markers and neuronal loss (Oakley et al., 2006). In contrast, 3xTg-AD mice show a slower progression of senile plaques and produce abnormal tau protein phosphorylation (Bilkei-Gorzo, 2014). As the principal research interest with 3xTg-AD mice lies in the interplay between senile plaques and neurofibrillary tangles, whereas with 5xFAD mice it's focused on A $\beta_{42}$ . This could explain why 5xFAD exhibits more severe cognitive and behavior tests at 4–5 months old. Initially, we intended to utilize 6–9 months old mice for our experiment. However, during the multi-channel recording phase, we encountered high mortality rates among these older mice. Also, the patch-clamp whole-cell recording from 6 to 9 months old mice was

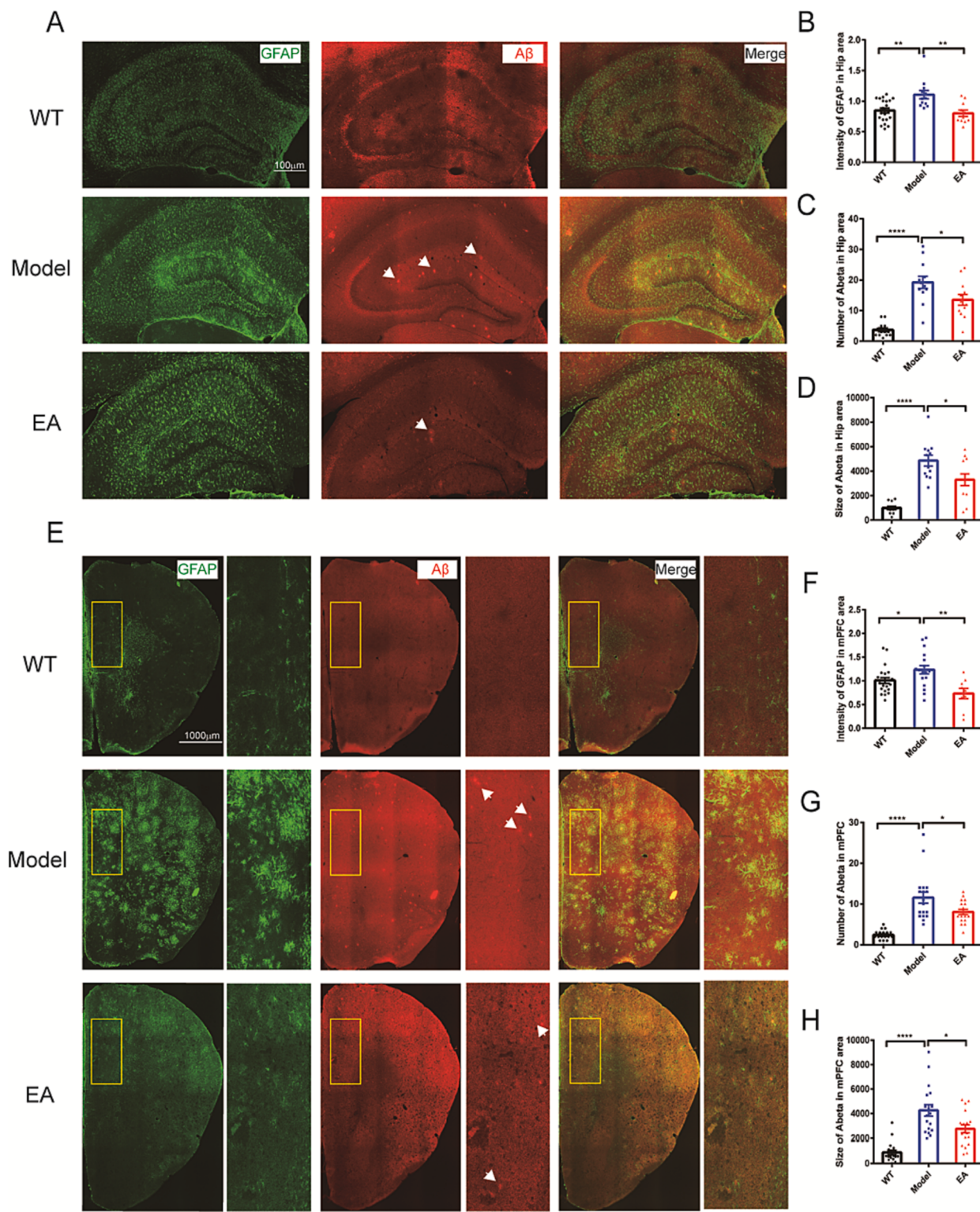
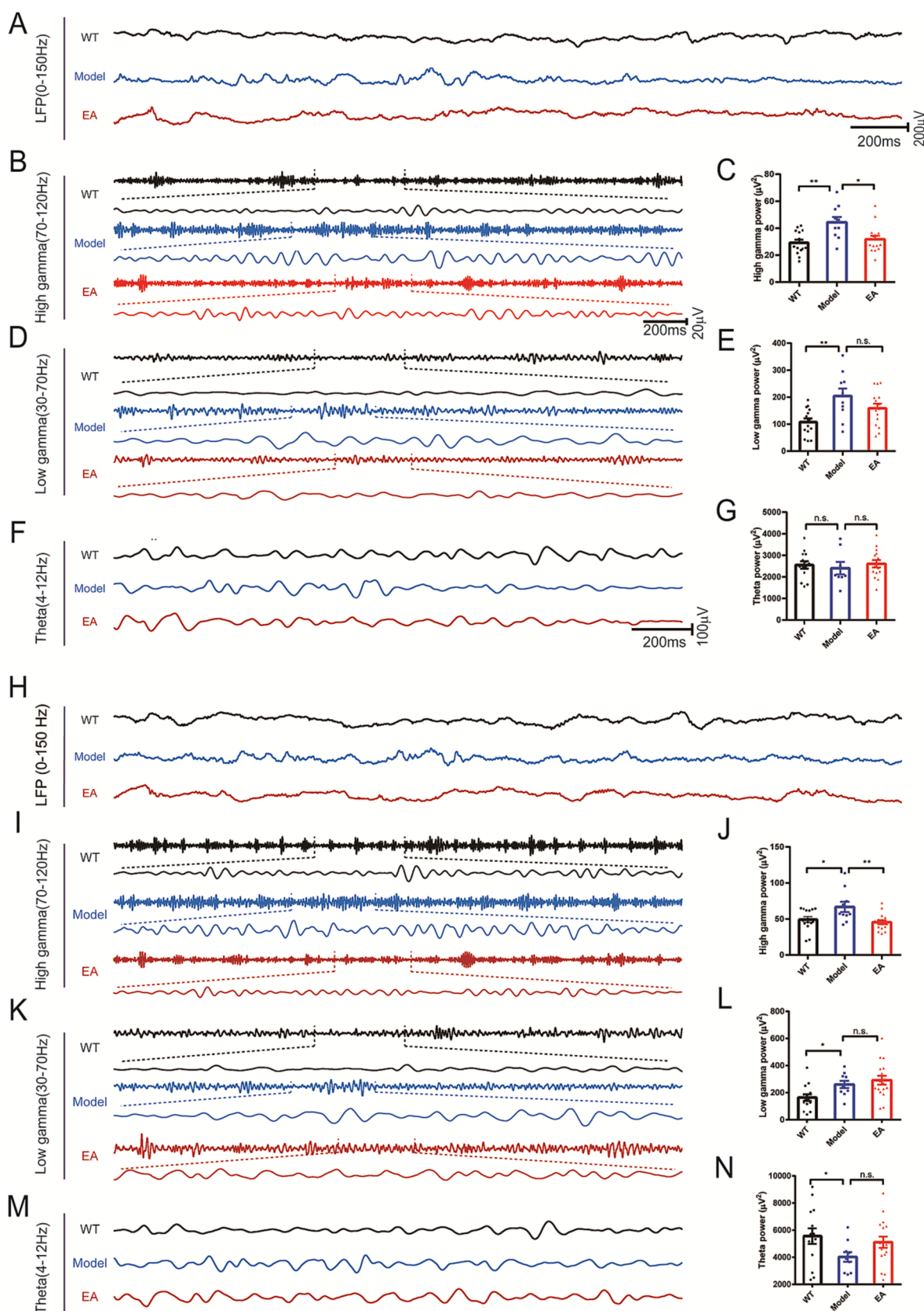


**Fig. 3.** EA reduced the amount of A $\beta$  in the brain of 5xFAD mice. (A) Hippocampal sections were stained to observe the activation of astrocytes (GFAP labeling) and the amount of A $\beta$ . (B) Analysis of GFAP staining results, in which EA reduced astrocyte activation in the hippocampus of 5xFAD mice (normalized). (C-D) Analysis of A $\beta$  staining results: EA reduced the number and size( $\mu\text{m}^2$ ) of A $\beta$  in the hippocampus of 5xFAD mice. (E) mpFC sections were stained to observe astrocyte activation (GFAP labeling) and A $\beta$  amount. (F) Analysis of GFAP staining results, in which EA reduced astrocyte activation in the mpFC region of 5xFAD mice (normalized). (G-H) Analysis of A $\beta$  staining results: EA reduced the number and size( $\mu\text{m}^2$ ) of A $\beta$  in the mpFC region of 5xFAD mice. All data are means  $\pm$  SEM. The number of images is indicated in bars. Statistical significance was assessed by unpaired two-tailed t-test (\* $P$  < 0.05, \*\* $P$  < 0.01, \*\*\*\* $P$  < 0.0001).



(caption on next page)

**Fig. 4.** EA reduced the high-frequency gamma oscillations in 5xFAD mice. **(A)** EA reduced the abnormal potentiation of LFP in the hippocampus of 5xFAD mice. **(B)** High gamma oscillations in the hippocampus of mice in each group. **(C)** Analysis of the results of High gamma oscillations in the hippocampus: EA reduced abnormally enhanced High gamma oscillations in the hippocampus of 5xFAD mice. **(D)** Low gamma oscillations in the hippocampus of mice in each group. **(E)** Analysis of the results of Low gamma oscillations in the hippocampus: EA did not affect abnormally enhanced Low gamma oscillations in the hippocampus of 5xFAD mice. **(F)** Theta oscillations in the hippocampus of mice in each group. **(G)** Theta oscillations in the hippocampus of 5xFAD mice did not change, and EA did not affect theta oscillations. **(H)** EA reduced the abnormal enhancement of LFP in the PFC region of 5xFAD mice. **(I)** High gamma oscillations in the PFC region of mice in each group. **(J)** Analysis of High gamma oscillation in the PFC region: EA reduced abnormally enhanced High gamma oscillation in the PFC region of 5xFAD mice. **(K)** Low gamma oscillations in the PFC region of mice in each group of mice. **(L)** Analysis of Low gamma oscillation in the PFC region: EA did not affect abnormally enhanced Low gamma oscillations in the PFC region of 5xFAD mice. **(M)** Theta oscillations in the PFC region of mice in each group. **(N)** Theta oscillations in the PFC region were reduced in 5xFAD mice, and EA did not affect theta oscillations. All data are means  $\pm$  SEM. The number of imagines is indicated in bars. Statistical significance was assessed by unpaired two-tailed *t*-test (\**P* < 0.05, \*\**P* < 0.01).

notably challenging. Given these difficulties, we opted for 4–5 months old mice for our experiments. To decide on the model showing more severe memory impairment, we conducted behavioral tests. Our results showed that the 5xFAD mice displayed more severe memory impairment, prompting us to select 5xFAD mice for our subsequent experiments.

A recent study revealed that a 40 Hz sound and light stimulation could effectively improve memory performance and reduce pathological levels of A $\beta$  in AD mice (Martorell et al., 2019). This finding inspired us to investigate the effects of 40 Hz EA treatment on the behavior of 5xFAD mice. Our results indicated that, akin to the sound and light stimulation, 40 Hz EA stimulation was capable of mitigating memory dysfunction, but it enhanced anxiety-like behaviors. Similarly, our results showed that 40 Hz EA stimulation also led to a decrease in both the number and size of A $\beta$  plaques in the hippocampus and mPFC region. Past studies showed that EA could inhibit the NF- $\kappa$ B pathway while activating the Stat6 pathway in microglia (Xie et al., 2021). The activation of the Stat6 pathway bolsters the phagocytic function of macrophages (Chen et al., 2021). Based on these observations, we speculate that EA's reduction of A $\beta$  plaques might be a result of the promotion of the phagocytic function of microglia. However, more thorough studies are required to substantiate this hypothesis.

The buildup of A $\beta$  is a defining characteristic of AD and has been shown to lead to synaptic dysfunction, neuron loss, and decreased connectivity between brain regions, which impacts higher cognitive functions and disrupts neural circuits (Canter et al., 2016). Meanwhile, regulation of abnormal neural activity has been shown to ease the pathological process of AD (Iaccarino et al., 2016). In our study, we focused on the effects of 40 Hz electrical stimulation (EA) on theta and gamma oscillations, which have been extensively studied due to their correlation with higher cognitive functions. Our findings indicated that EA exerted its effects primarily by regulating high gamma oscillation, but not low gamma oscillation or theta oscillation. In contrast to prior studies, we discovered that gamma oscillation in 5xFAD mice was weaker than in wild-type mice, and EA effectively restored the abnormally high oscillation to normal levels. There are two possible explanations for this difference: (1) The reduction of the number and size of A $\beta$  plaques in the prefrontal cortex and hippocampus might not have been achieved solely through the regulation of abnormal gamma oscillations; (2) EA could also modulate both theta and gamma oscillations and boost the phagocytic function of astrocytes to remove A $\beta$  plaques.

The exact mechanism by which 40 Hz EA reduces high gamma oscillation remains elusive and warrants further investigation. Rapid oscillations of neurons are believed to be driven by neural networks, with astrocytes playing a crucial role in generating gamma oscillation. An increase in calcium levels in astrocytes triggers the release of neurotransmitters (Mahmoud et al., 2019); and blocking the release of neurotransmitters weakens gamma oscillation by preventing astrocytes from communicating with nearby cells (Lee et al., 2014). Our findings showed that EA could inhibit the activation of astrocytes, but we are still in the dark about how EA affects neurotransmitter release by astrocytes. Given that previous studies have reported the regulation of astrocytes by EA, we speculate that EA reduces gamma oscillation by inhibiting neurotransmitter release by astrocytes. More studies are needed to verify

this hypothesis.

Additionally, we examined the synaptic function of neurons in the hippocampus and mPFC regions. It is worth noting that EA enhances the amplitude of EPSCs, particularly those mediated by AMPA. AMPA receptors are a type of ionotropic glutamate receptor that enable fast excitatory neurotransmission. Dysfunction of AMPA receptors is associated with the presence of soluble A $\beta$  (Baglietto-Vargas et al., 2018). A $\beta$  can bind with the C-tail of GluA2 (Zhao et al., 2010), leading to the internalization of AMPA receptors and resulting in synaptic modifications (Passafaro et al., 2003; Zhang et al., 2018). High concentrations of soluble oligomeric A $\beta$  can also trigger constant endocytosis and removal of AMPA receptors (Guntupalli et al., 2017). The cognitive impairments induced by A $\beta$  can also be alleviated after inhibiting the endocytosis of GluA2/AMPA receptors (Ashourpour et al., 2022). Hence, we hypothesize that the clearance of A $\beta$  plaques following EA stimulation may be responsible for the improvement in the amplitude of AMPA-mediated EPSCs. This aligns with the two possible reasons mentioned earlier, suggesting that the primary cause for the improvement in memory impairment by EA may not be directly related to neural electrical activity, despite their intimate connection.

In our study, we explored the effect of EA on neuronal electrical activity, but there is still substantial room for further exploration. Future research needs to address the following limitations:

1. Elucidating how EA influences astrocyte activity, which could provide insights into why EA reduces high gamma oscillation.
2. Investigating whether EA augments the phagocytic ability of astrocytes, which could help explain the reduction in A $\beta$  plaques.
3. Determining the molecular target of EA. We observed that EA enhances both mIPSC and mEPSC in the hippocampus and mPFC regions, but the underlying mechanisms are yet to be understood. A spatial transcriptome analysis will be performed to identify the differentially expressed genes in astrocytes and neurons.

## 6. Ethical approval and consent to participate

All animal experiments and protocols complied with international animal experimental ethics and requirements, and were approved by the Animal Ethics Committee of Guangzhou University of Chinese Medicine (Permit No. XMULAC20210062).

## 7. Consent for publication

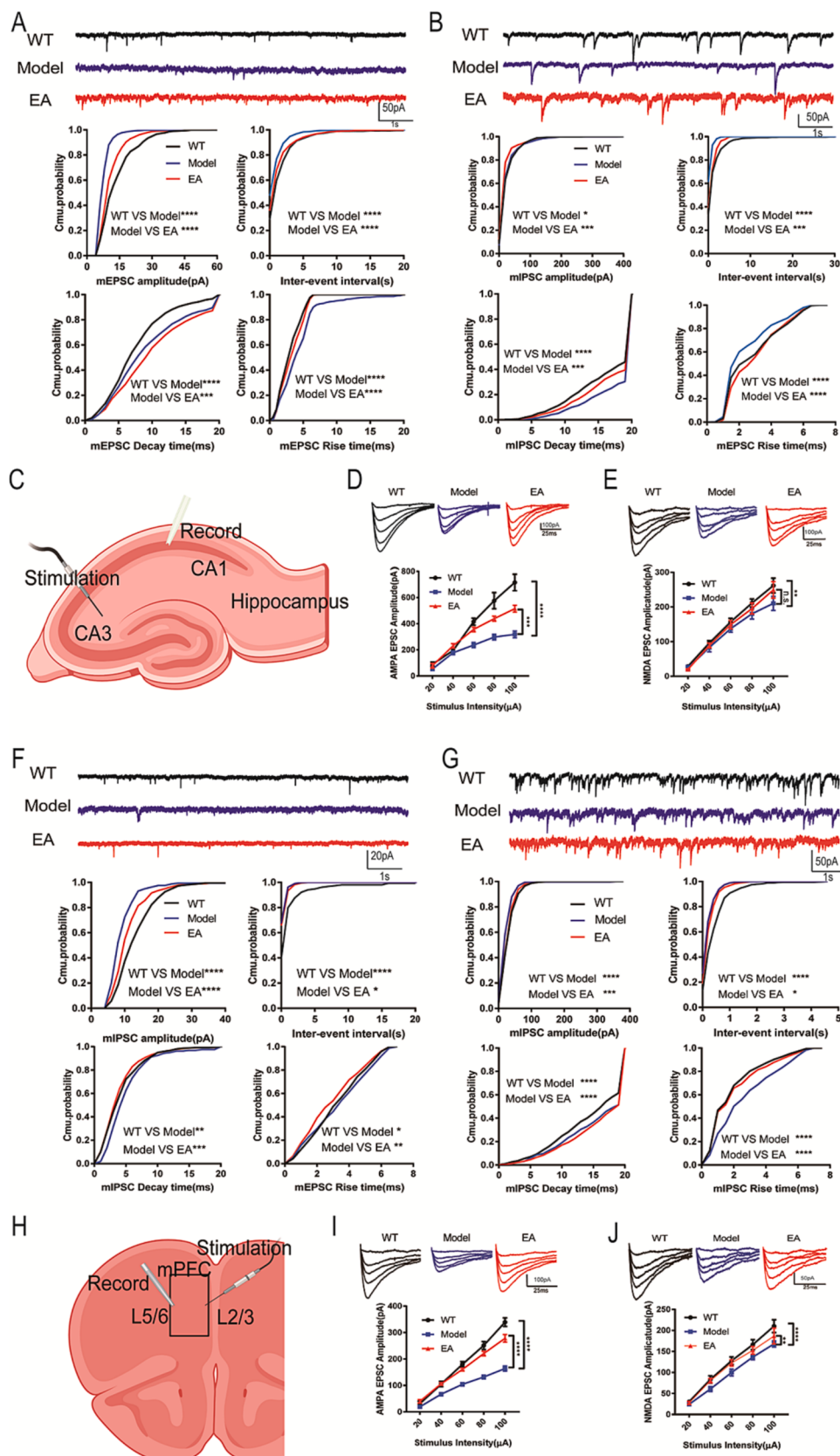
Not applicable.

## 8. Availability of data and materials

The raw data and materials applied in the study will be available for all qualified researchers without any reservation.

## Funding

This work was supported by China Postdoctoral Science Foundation, grant number: 2021 M700223.



*(caption on next page)*

**Fig. 5.** EA enhanced synaptic transmission in the brains of 5xFAD mice. **(A)** EA increased the amplitude, frequency, and decay time of mEPSC in hippocampal pyramidal neurons of 5xFAD mice, but decreased the rise time, n = 13. **(B)** EA increased the frequency and rise time of mIPSC, but decreased the amplitude and decay time in hippocampal pyramidal neurons of 5xFAD mice, n = 14. **(C)** Schematic diagram of eEPSC recording in the hippocampus. **(D)** EA enhanced AMPA-mediated EPSC intensity in the hippocampus of 5xFAD mice, n = 17. **(E)** EA did not affect NMDA-mediated EPSC intensity in the hippocampus of 5xFAD mice, n = 14. **(F)** EA increased the amplitude and frequency, and decreased the decay time and rise time of mEPSC in pyramidal neurons in the mPFC region of 5xFAD mice, n = 8. **(G)** EA increased the amplitude, frequency, and decay time, and decreased the rise time of mIPSC in pyramidal neurons in the mPFC region of 5xFAD mice, n = 11. **(H)** Schematic diagram of eEPSC recordings in the mPFC region. **(I)** EA enhanced AMPA-mediated EPSC intensity in the mPFC region of 5xFAD mice, n = 14. **(J)** EA enhanced NMDA-mediated EPSC intensity in the mPFC region of 5xFAD mice, n = 14. All data are means  $\pm$  SEM. The number of imagines is indicated in bars. Statistical significance was assessed by two-way ANOVA or Kolmogorov-Smirnov test (\* $P < 0.05$ , \*\* $P < 0.01$ , \*\*\* $P < 0.001$ , \*\* $P < 0.0001$ ).

## 10. Authors' contributions

Every author participated in the designing, conduction and data collection of the study. Jifei Miao and Jiao Lan write the draft manuscript.

## Declaration of Competing Interest

The authors declare that they have no known competing financial interests or personal relationships that could have appeared to influence the work reported in this paper.

## Data availability

Data will be made available on request.

## References

- Arroyo-García, L.E., Isla, A.G., Andrade-Talavera, Y., Balleza-Tapia, H., Loera-Valencia, R., Alvarez-Jimenez, L., Pizzirusso, G., Tambaro, S., Nilsson, P., Fisahn, A., 2021. Impaired spike-gamma coupling of area CA3 fast-spiking interneurons as the earliest functional impairment in the App(NL-G-F) mouse model of Alzheimer's disease. *Mol. Psychiatry* 26, 5557–5567. <https://doi.org/10.1038/s41380-021-01257-0>.
- Ashourpour, F., Jafari, A., Babaei, P., 2022. Co-treatment of AMPA endocytosis inhibitor and GluN2B antagonist facilitate consolidation and retrieval of memory impaired by  $\beta$  amyloid peptide. *Int. J. Neurosci.* 132, 714–723. <https://doi.org/10.1080/00207454.2020.1837800>.
- Baglietto-Vargas, G.A., Prieto, A., Limon, S., Forner, C.J., Rodriguez-Ortiz, K., Ikemura, R., R. Ager, R., Medeiros, L., Trujillo-Estrada, A.C., Martini, M., Kitazawa, J.C., Davila, C.W., Cotman, A., Gutierrez, F.M., LaFerla, Impaired AMPA signaling and cytoskeletal alterations induce early synaptic dysfunction in a mouse model of Alzheimer's disease. *Aging Cell* 17 (2018) e12791. <https://doi.org/10.1111/acel.12791>.
- Bilkei-Gorzo, A., 2014. Genetic mouse models of brain ageing and Alzheimer's disease. *Pharmacol. Ther.* 142, 244–257. <https://doi.org/10.1016/j.pharmthera.2013.12.009>.
- Bustos, V., Pulina, M.V., Ledo, J., 2021. Amyloidogenic and anti-amyloidogenic properties of presenilin 1. *Adv. Pharmacol.* 90, 239–251. <https://doi.org/10.1016/b.sapha.2020.09.010>.
- Canter, R.G., Penney, J., Tsai, L.-H., 2016. The road to restoring neural circuits for the treatment of Alzheimer's disease. *Nature* 539, 187–196. <https://doi.org/10.1038/nature20412>.
- Chen, M., Tse, G., Wong, W.T., 2021. Interleukin-4 increases phagocytosis of necrotic cells by macrophages through scavenger receptor CD36. *Clin. Exp. Pharmacol. Physiol.* 48 (1), 129–136.
- Colom-Cadena, M., Spires-Jones, T., Zetterberg, H., Blennow, K., Caggiano, A., Dekosky, S.T., Fillit, H., Harrison, J.E., Schneider, L.S., Scheltens, P., De Haan, W., Grundman, M., Van Dyck, C.H., Izzo, N.J., Catalano, S.M., 2020. The clinical promise of biomarkers of synapse damage or loss in Alzheimer's disease. *Alzheimer's Res. Ther.* 12, 1–12. <https://doi.org/10.1186/s13195-020-00588-4>.
- D'Amelio, M., Cavallucci, V., Middei, S., Marchetti, C., Pacioni, S., Ferri, A., Diamantini, A., De Zio, D., Carrara, P., Battistini, L., Moreno, S., Bacci, A., Ammassari-Teule, M., Marie, H., Cecconi, F., 2011. Caspase-3 triggers early synaptic dysfunction in a mouse model of Alzheimer's disease. *Nat. Neurosci.* 14, 69–76. <https://doi.org/10.1038/nn.2709>.
- Diociaiuti, M., Bonanni, R., Cariati, I., Frank, C., D'Arcangelo, G., 2021. Amyloid Prefibrillar Oligomers: The Surprising Commonalities in Their Structure and Activity. *Int. J. Molecul. Sci.* 22, 6435. <https://doi.org/10.3390/ijms22126435>.
- Doelling, K.B., Assaneo, M.F., 2021. Neural oscillations are a start toward understanding brain activity rather than the end. *PLoS Biology* 19, e3001234.
- Etter, G., van der Veldt, S., Manseau, F., Zarrinkoub, I., Trillaud-Doppia, E., Williams, S., 2019. Optogenetic gamma stimulation rescues memory impairments in an Alzheimer's disease mouse model. *Nat. Commun.* 10, 5322. <https://doi.org/10.1038/s41467-019-13260-9>.
- Guntupalli, S., Jang, S.E., Zhu, T., Huganir, R.L., Widagdo, J., Anggono, V., 2017. GluA1 subunit ubiquitination mediates amyloid- $\beta$ -induced loss of surface  $\alpha$ -amino-3-hydroxy-5-methyl-4-isoxazolepropionic acid (AMPA) receptors. *J. Biol. Chem.* 292, 8186–8194. <https://doi.org/10.1074/jbc.M116.774554>.
- He, Y., Wei, M., Wu, Y., Qin, H., Li, W., Ma, X., Cheng, J., Ren, J., Shen, Y., Chen, Z., Sun, B., Huang, F.-D., Shen, Y., Zhou, Y.-D., 2019. Amyloid  $\beta$  oligomers suppress excitatory transmitter release via presynaptic depletion of phosphatidylinositol-4,5-bisphosphate. *Nat. Commun.* 10, 1193. <https://doi.org/10.1038/s41467-019-09114-z>.
- Iaccarino, H.F., Singer, A.C., Martorell, A.J., Rudenko, A., Gao, F., Gillingham, T.Z., Mathys, H., Seo, J., Kritskiy, O., Abdurrob, F., Adaikan, C., Canter, R.G., Rueda, R., Brown, E.N., Boyden, E.S., Tsai, L.-H., 2016. Gamma frequency entrainment attenuates amyloid load and modifies microglia. *Nature* 540, 230–235. <https://doi.org/10.1038/nature20587>.
- Lanté, F., Chafai, M., Raymond, E.F., Pereira, A.R.S., Mouska, X., Kootar, S., Barik, J., Bethus, I., Marie, H., 2015. Subchronic glucocorticoid receptor inhibition rescues early episodic memory and synaptic plasticity deficits in a mouse model of Alzheimer's disease. *Neuropsychopharmacology* 40, 1772–1781. <https://doi.org/10.1038/npp.2015.25>.
- Lee, H.S., Ghetti, A., Pinto-Duarte, A., Wang, X., Dziewczapski, G., Galimi, F., Huitron-Resendiz, S., Piña-Crespo, J.C., Roberts, A.J., Verma, I.M., Sejnowski, T.J., Heinemann, S.F., 2014. Astrocytes contribute to gamma oscillations and recognition memory. *Proc. Natl. Acad. Sci. of the United States of America* 111, E3343–E3352. <https://doi.org/10.1073/pnas.1410893111>.
- Mahmoud, S., Gharagozloo, M., Simard, C., Gris, D., 2019. Astrocytes Maintain Glutamate Homeostasis in the CNS by Controlling the Balance between Glutamate Uptake and Release. *Cells* 8 (2), 184.
- Martorell, A.J., Paulson, A.L., Suk, H.-J., Abdurrob, F., Drummond, G.T., Guan, W., Young, J.Z., Kim, D.-N.-W., Kritskiy, O., Barker, S.J., Mangena, V., Prince, S.M., Brown, E.N., Chung, K., Boyden, E.S., Singer, A.C., Tsai, L.-H., 2019. Multi-sensor Gamma Stimulation Ameliorates Alzheimer's-Associated Pathology and Improves Cognition. *Cell* 177, 256–271. <https://doi.org/10.1016/j.cell.2019.02.014>.
- Oakley, H., Cole, S.L., Logan, S., Maus, E., Shao, P., Craft, J., Guillozet-Bongaarts, A., Ohno, M., Disterhoff, J., Van Eldik, L., Berry, R., Vassar, R., 2006. Intraneuronal beta-amyloid aggregates, neurodegeneration, and neuron loss in transgenic mice with five familial Alzheimer's disease mutations: potential factors in amyloid plaque formation. *J. Neurosci.* 26, 10129–10140. <https://doi.org/10.1523/JNEUROSCI.1202-06.2006>.
- Parhizkar, S., Holtzman, D.M., 2022. APOE mediated neuroinflammation and neurodegeneration in Alzheimer's disease. *Semin. Immunol.* 26, 101594. <https://doi.org/10.1016/j.smim.2022.101594>.
- Passafaro, M., Nakagawa, T., Sala, C., Sheng, M., 2003. Induction of dendritic spines by an extracellular domain of AMPA receptor subunit GluR2. *Nature* 424, 677–681. <https://doi.org/10.1038/nature01781>.
- Peng, L., Bestard-Lorigados, I., Song, W., 2022. The synapse as a treatment avenue for Alzheimer's Disease. *Mol. Psychiatry* 27, 2940–2949. <https://doi.org/10.1038/s41380-022-01565-z>.
- Ruiter, M., Herstel, L.J., Wierenga, C.J., Ma, T., 2020. Reduction of Dendritic Inhibition in CA1 Pyramidal Neurons in Amyloidosis Models of Early Alzheimer's Disease. *J. Alzheimers Dis.* 78 (3), 951–964.
- Scheltens, P., De Strooper, B., Kivipelto, M., Holstege, H., Chételat, G., Teunissen, C.E., Cummings, J., Van Der Flier, W.M., 2022. Alzheimer's disease. *Lancet* 397, 1577–1590. [https://doi.org/10.1016/S0140-6736\(20\)32205-4](https://doi.org/10.1016/S0140-6736(20)32205-4). Alzheimer.
- Sevigny, J., Chiao, P., Bussière, T., Weinreb, P.H., Williams, L., Maier, M., Dunstan, R., Salloway, S., Chen, T., Ling, Y., O'Gorman, J., Qian, F., Arastu, M., Li, M., Chollate, S., Brennan, M.S., Quintero-Monzon, O., Scannevin, R.H., Arnold, H.M., Engber, T., Rhodes, K., Ferrero, J., Hang, Y., Mikulskis, A., Grimm, J., Hock, C., Nitsch, R.M., Sandrock, A., 2016. The antibody aducanumab reduces  $\beta$ A<sub>1</sub> plaques in Alzheimer's disease. *Nature* 537, 50–56. <https://doi.org/10.1038/nature19323>.
- Tang, Y., Shao, S., Guo, Y., Zhou, Y., Cao, J., Xu, A., Wu, J., Li, Z., Xiang, D., 2019. Electroacupuncture Mitigates Hippocampal Cognitive Impairments by Reducing BACE1 Deposition and Activating PKA in APP/PS1 Double Transgenic Mice. *Neural Plast.* 4, 2823679. <https://doi.org/10.1155/2019/2823679>.
- van Dyck, C.H., 2018. Anti-Amyloid- $\beta$  Monoclonal Antibodies for Alzheimer's Disease: Pitfalls and Promise. *Biol. Psychiatry* 83, 311–319. <https://doi.org/10.1016/j.biopsych.2017.08.010>.
- Xiao, L.-Y., Wang, X.-R., Yang, J.-W., Ye, Y., Zhu, W., Cao, Y., Ma, S.-M., Liu, C.-Z., 2018. Acupuncture Prevents the Impairment of Hippocampal LTP Through  $\beta$ 1-AR in Vascular Dementia Rats. *Mol. Neurobiol.* 55, 7677–7690. <https://doi.org/10.1007/s12035-018-0943-x>.
- Xie, L., Liu, Y.i., Zhang, N., Li, C., Sandhu, A.F., Williams, G., Shen, Y., Li, H., Wu, Q., Yu, S., 2021. Electroacupuncture Improves M2 Microglia Polarization and Glia Anti-inflammation of Hippocampus in Alzheimer's Disease. *Front. Neurosci.* 15, 689629. <https://doi.org/10.3389/fnins.2021.689629>.
- Xu, A., Zeng, Q., Tang, Y., Wang, X., Yuan, X., Zhou, Y., Li, Z., 2020. Electroacupuncture Protects Cognition by Regulating Tau Phosphorylation and Glucose Metabolism via

- the AKT/GSK3 $\beta$  Signaling Pathway in Alzheimer's Disease Model Mice. *Front. Neurosci.* 14, 585476. <https://doi.org/10.3389/fnins.2020.585476>.
- Yang, G., Pei, Y.-N., Shao, S.-J., Gao, Y.-S., Zhang, S.-J., Hu, C., Feng, S.-N., Xue, W.-G., 2020. [Effects of electroacupuncture at "Baihui" and "Yongquan" on the levels of synaptic plasticity related proteins postsynaptic density-95 and synaptophysin in hippocampus of APP/PS1 mice]., Zhen ci yan jiu = Acupunct. Philos. Phenomenol. Res. 45, 310–314. <https://doi.org/10.13702/j.1000-0607.190012>.
- Ye, Y., Li, H., Yang, J.-W., Wang, X.-R., Shi, G.-X., Yan, C.-Q., Ma, S.-M., Zhu, W., Li, Q.-Q., Li, T.-R., Xiao, L.-Y., Liu, C.-Z., 2017. Acupuncture Attenuated Vascular Dementia-Induced Hippocampal Long-Term Potentiation Impairments via Activation of D1/D5 Receptors. *Stroke* 48, 1044–1051. <https://doi.org/10.1161/STROKEAHA.116.014696>.
- Zhang, Y., Guo, O., Huo, Y., Wang, G., Man, H.-Y., Ma, T., 2018. Amyloid- $\beta$  Induces AMPA Receptor Ubiquitination and Degradation in Primary Neurons and Human Brains of Alzheimer's Disease. *J. Alzheimers Dis.* 62 (4), 1789–1801.
- Zhao, J., Liu, X., Xia, W., Zhang, Y., Wang, C., 2020. Targeting Amyloidogenic Processing of APP in Alzheimer's Disease. *Front. Mol. Neurosci.* 13, 137. <https://doi.org/10.3389/fnmol.2020.00137>.
- Zhao, W.-Q., Santini, F., Breese, R., Ross, D., Zhang, X.D., Stone, D.J., Ferrer, M., Townsend, M., Wolfe, A.L., Seager, M.A., Kinney, G.G., Shughrue, P.J., Ray, W.J., 2010. Inhibition of calcineurin-mediated endocytosis and alpha-amino-3-hydroxy-5-methyl-4-isoxazolepropionic acid (AMPA) receptors prevents amyloid beta oligomer-induced synaptic disruption. *J. Biol. Chem.* 285, 7619–7632. <https://doi.org/10.1074/jbc.M109.057182>.
- Zheng, Q., Kong, L.-H., Yu, C.-C., He, R.-Y., Wang, X.-S., Jiang, T., Ma, R., Chen, Y.-Y., Wang, Y.-S., 2020. [Effects of electroacupuncture on cognitive function and neuronal autophagy in rats with D-galactose induced Alzheimer's disease]., Zhen ci yan jiu = Acupunct. Philos. Phenomenol. Res. 45, 689–695. <https://doi.org/10.13702/j.1000-0607.190854>.
- Zheng, X., Lin, W., Jiang, Y., Lu, K., Wei, W., Huo, Q., Cui, S., Yang, X., Li, M., Xu, N., Tang, C., Song, J.-X., 2021. Electroacupuncture ameliorates beta-amyloid pathology and cognitive impairment in Alzheimer disease via a novel mechanism involving activation of TFEB (transcription factor EB). *Autophagy* 17, 3833–3847. <https://doi.org/10.1080/15548627.2021.1886720>.